Hindawi
Adsorption Science & Technology
Volume 2022, Article ID 4659410, 12 pages
https://doi.org/10.1155/2022/4659410

Research Article

Surface Characteristics of Electrospun *p*-Sulphonated Calix[4]Arene Functionalized Cellulose Acetate Nanofiber and Its Behaviour towards Methylene Blue Adsorption

Nur Amilah Fadlina Basri,[1] **Mohd Haniff Wahid**,[1] **Zulkarnain Zainal**,[1,2] **Shahrul Ainliah Alang Ahmad**,[1] **and Mohd Rashidi Abdull Manap**[1]

[1]*Department of Chemistry, Faculty of Science, Universiti Putra Malaysia, 43400, UPM, Serdang, Selangor Darul Ehsan, Malaysia*
[2]*Nanomaterials Synthesis and Characterisation Laboratory, Institute of Nanoscience and Nanotechnology, Universiti Putra Malaysia, 43400, UPM, Serdang, Selangor Darul Ehsan, Malaysia*

Correspondence should be addressed to Mohd Haniff Wahid; mw_haniff@upm.edu.my

Received 17 May 2022; Revised 6 October 2022; Accepted 11 October 2022; Published 9 December 2022

Academic Editor: Muhammad Raziq Rahimi Kooh

p-sulphonated calix[4]arene (*p*-SOCX) functionalized cellulose acetate/graphene oxide (CA/GO) nanofibers were successfully prepared via the electrospinning technique. The presence of *p*-SOCX within the fiber matrix was ascertained using Fourier Transform Infrared spectroscopy and Carbon-Hydrogen-Nitrogen-Sulphur elemental analyses. Apparent changes in morphology of the samples were observed under scanning electron microscope where fiber diameters increased with increasing *p*-SOCX content. Preliminary dye removal test at different pH, dosage, and temperature of functionalized CA/GO nanofiber demonstrates enhanced adsorption capacity of methylene blue in presence of *p*-SOCX compared to pristine CA nanofiber and CA/GO nanofiber at an optimum pH 8. The highest removal efficiency obtained was 88.84% with initial methylene blue dye concentration of 10 mg/L, adsorbent dosage of 20 mg/10 mL, contact time of 30 min at room temperature *ca.* 293 K.

1. Introduction

There is a major global concern on water quality. The increasing demand for organic dyes in industrial activities, namely, textile, cosmetic, tanning, and others has resulted in large quantities of dye released to the environment [1]. Methylene blue (MB) dye, which is cationic, is mainly used for dyeing cotton, wool, and silk and is also used in medical applications as a chromophore due to its polar characteristic and strong resistance towards biodegradation [2, 3]. Nevertheless, continuous exposure to MB may lead to health issues such as mental confusion, vomiting, eye burn, shock, and increased heartbeat rate [4]. Due to its relevance and wide range of applications, MB, a member of the thiazine dye class, is chosen as the targeted dye for this investigation [5]. To date, various technologies such as membrane filtration, flocculation, chemical oxidation, ozonation, ion exchange, irradiation, and adsorption has been explored [6]. However, most of these methods have disadvantages such as lack of reusability which may hinder their widespread usage for large scale operations [7]. Meanwhile, adsorption technique offers advantages such as low development cost, easy to handle, and simple design [8].

Utilizing source abundant materials for dye removal such as cellulose acetate, CA as an adsorbent is preferred, however, its application in wastewater treatment is hampered due to the limited adsorption capacity of pristine CA. Several studies reported that, by grafting the fibers with functional groups of carboxyl (-COOH), amine ($-NH_2$), and sulfonate ($-SO_3H$) and also by addition of graphene oxide (GO), the dye adsorption capability can be enhanced [7]. The latter, i.e., GO, is endowed with oxygen-rich functional groups, which is readily modifiable via organic chemistry, and also possess other traits such as better stability, antifouling, and hydrophilic, which are ideal for the development of an excellent adsorbent [9].

Calixarene's are dubbed as third-generation macromolecules after crown ethers and cyclodextrins [10]. They have received considerable attention due to their unique structure of three-dimensional (3D) cavity-type which are made up of phenolic units linked by methylene bridges with upper and lower rims that can be chemically tailored. Such structures are preferable to be used as molecular platforms having selective interaction with cations, anions, or neutral molecules [11, 12]. Furthermore, presence of benzene rings renders calixarenes effective for benzene-based pollutants extraction such as MB and others [13]. Calixarene's unique conformation and complexation properties lend well in studies of synthetic, natural hosts, and the water treatment industry [10]. Nevertheless, novel composites materials from calixarenes are also being developed so as to extend its widespread applications resulting in various uses such as luminescent probes, solid phase extractants, adsorbents, catalyst, and sensor [7]. Noteworthy mentioning, majority of calixarenes are soluble only in nonpolar organic solvents such as toluene and chloroform, thus are nonenvironmentally friendly. On the other hand, water soluble calixarenes are more environmentally friendly and feasible for functionalization, thus we have selected *p*-sulfonated calixarene to use in this study (Figure 1).

Lafi et al., reported that by incorporating calix[8]arene into PAN nanofibers (C/PAN) [8] for the removal of Congo red and neutral red, it exhibited good stability and convenient recovery [14]. Moreover, PAN nanofibers containing calixarenes bearing N-methylglucamine functional groups (Calix-NMG/PAN) were reported as efficient adsorbents to remove chromate anions and uranium cations. The said composite provides higher ion binding ability due to high surface area, porosity, flexibility, and microporosity of PAN nanofibers with calixarene molecules containing N-methylglucamine as a chelating group [15]. There are also adsorption studies reported involving porous covalent calix[4]arene-based polymer towards cationic dyes namely, MB and rhodamine B, which exhibits maximal adsorption capacities of 625 mg/g and 484 mg/g, respectively [7]. This proves that calixarene has potential towards cationic ion removal [15].

The primary goal of this study is to utilize calixarene and graphene oxide to develop a novel composite cellulose-based nanofiber and to assess the adsorption behavior and critical analytical variables affecting the adsorption effectiveness of newly synthesized nanofibrous mat of CA/GO with *p*-SOCX toward the carcinogenic MB dye from aqueous environment. Nanofibers possess characteristics such as high surface area and high volume to mass ratio thus have been favored in water or wastewater treatment [16, 17]. An effective method for preparing nanofibers from a wide range of polymers in different shapes is known as electrospinning. Since nanofibers are affordable from a range of polymers, polymer blends, sol-gels, suspensions, emulsions, and composite structures, this technology offers a remarkable advantage over conventional manufacturing procedures [18]. The prepared composite material was thoroughly characterized using FT-IR, SEM, TGA, XRD, CHNS, and the operating parameters for dye removal from aqueous solution was studied.

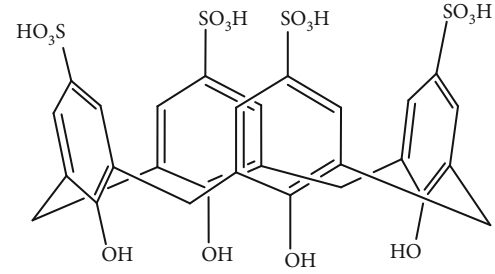

Figure 1: Chemical structure of calix[4]arene bearing sulphonate groups on the upper-rim.

2. Experimental

2.1. Material. CA (M.W.: 264.23 g/mol, 29-45%) and acetone (M.W.:58.08 g/mol, 99.5%) were supplied by R&M Chemicals, Malaysia. N, N-dimethylformamide (M.W.:73.09 g/mol, 99.9%) was purchased from Chemiz, Malaysia while GO and *p*-SOCX (M.W.: 744.74 g/mol, 4-10% edge-oxidized) were obtained from Sigma-Aldrich. MB (M.W.: 319.00 g/mol, 96%) was purchased from BDH Laboratory supplies. Sodium hydroxide (NaOH, M.W.: 40.00 g/mol, 99%) and hydrochloric acid (HCl, 37%) was purchased from Merck. Distilled water was used throughout the experiments.

2.2. Preparation of Cellulose Acetate/Graphene Oxide/p-Sulphonated Calix[4]Arene (CA/GO/SOCX) Nanofiber. 1 g of CA was first dissolved in an acetone and DMF mixture solvent system until a clear solution was obtained. Next, 0.05 g of GO and 1%, 3%, and 5% of *p*-SOCX were added into the solution and mixture was left until complete dissolution. A 10 mL syringe was then used to feed the mixture solution shown in Figure 2 for the fiber-making step via electrospinning. A collector plate covered with aluminium foil was used as a substrate to collect the electrospun nanofibers shown in Figure 2. The operating voltage was set to 19 kV with flow rate of 2.0 mL/h. The distance between the nanofiber collector and the tip of the needle was fixed at 10 cm.

2.3. Physicochemical Characterization of Adsorbents. FTIR measurements were carried out using an Alpha II, Bruker spectrometer equipped with a platinum diamond ATR module, ZnSe beam splitter, and a RT-DLaTGS detector. The transmission spectra were recorded between 550 and 4000 cm^{-1} with a spectral resolution of 4 cm^{-1} accumulating 32 scans. Elemental analysis of the nanofibers obtained was performed using carbon-hydrogen-nitrogen-sulphur (CHNS) analyzer TruSpec® micro, Leco, U.S. Morphological study of the nanofibers was carried out using JEOL, JSM-IT100 InTouchScope™ scanning electron microscope with 10 kV accelerating voltage and working distance of 12 mm. MB absorbance was determined using UV-*Vis* spectrometer Perkin Elmer SPS 1063 while pH was monitored using a pH meter (CyberScan 500, Eutech Instruments). The crystal phases and structure of all samples were identified by X-ray diffraction (XRD, Shimadzu Model XRD-6000) at 2θ range from 20° to 50° with scanning rate of 2°/min [19]. Meanwhile, the weight loss of nanofibers was measured using thermal gravimetric

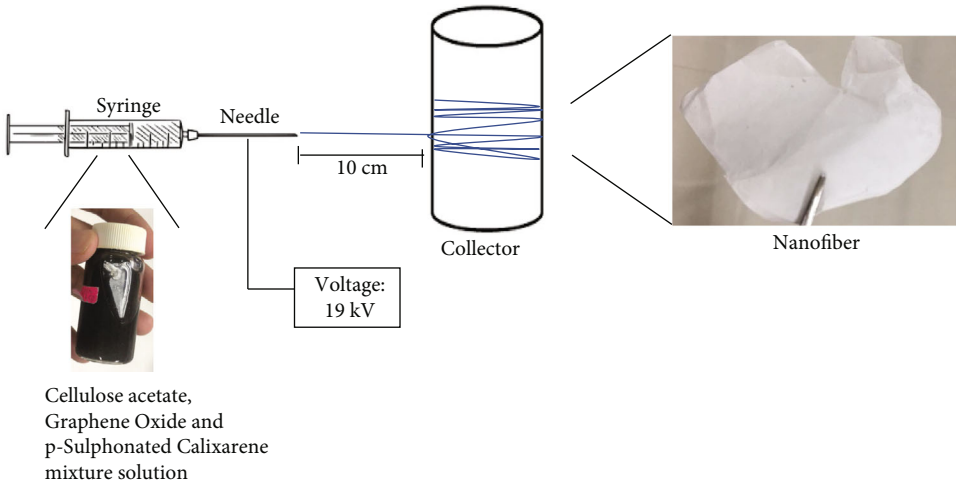

Figure 2: Schematic diagram of the nanofiber preparation using electrospinning setup.

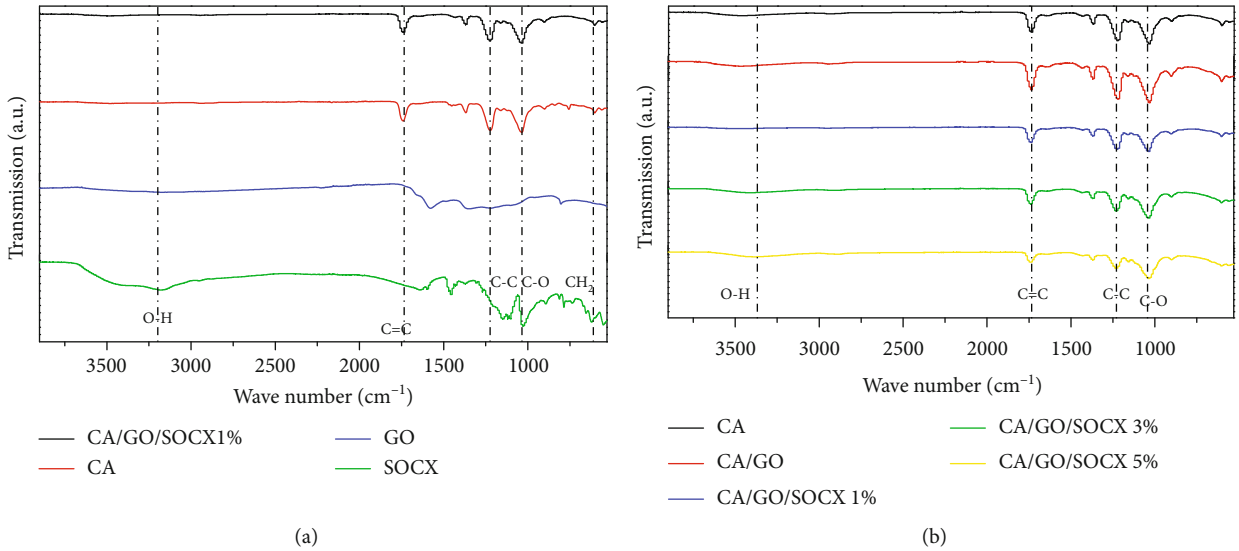

Figure 3: (a) FTIR spectra of starting material CA, GO, SOCX, and combined CA functionalized GO with 1% p-SOCX, (b) FTIR spectra of nanofibers of CA, GO functionalized CA, and GO functionalized CA with different amount of p-SOCX (1%, 3% and 5%).

analysis (TGA), using Mettler Toledo Thermogravimetric Model (TGA/SDTA-851e/STARe). The samples were cut into small pieces and heated to temperatures between 50°C to 700°C in nitrogen atmosphere, and weight loss was recorded.

2.4. Dye Removal Study. MB stock solution was prepared by first dissolving 1 g of MB into 1 L of deionized water followed by dilution to different concentrations ranging from 10 ppm to 100 ppm. A calibration curve was then established at the absorbance of 664 nm. Adsorption study was conducted in batch mode at different conditions, i.e., pH, dosage, and temperature. The pH effect towards MB adsorption was investigated between pH 7 to pH 10 by adjusting the pH of the dye solution using 0.1 M HCl or 0.1 M NaOH and adsorbent dosage was varied from 6 mg to 30 mg while the temperature studies was carried out between 293 K to 353 K. All experiments were repeated 3 times each.

Prior to the MB removal test, pH value at the point of zero charge (pH_{PZC}) of the nanofiber samples was investigated using the salt addition method which involves 0.025 g of adsorbent in 10 mL of 0.01 M sodium nitrate ($NaNO_3$) at pH values of 5, 7, 8, 9, and 10 and were left overnight. The pH_{PZC} value was then plotted from the ΔpH ($pH_{final} - pH_{initial}$) versus the initial pH where the intersection of the curve and the pH_0 axis denotes the pH_{PZC} [3]. Meanwhile, MB concentration and volume was fixed at 10 ppm and 10 mL, respectively. The residual methylene blue concentration was determined using UV-*Vis* spectrometer using the same method outlined earlier. Adsorption capacity, q_e and percentage removal, %R were then calculated using Equations (1) and (2) consecutively.

$$q_e : \frac{(C_o - C_e)V}{m}, \quad (1)$$

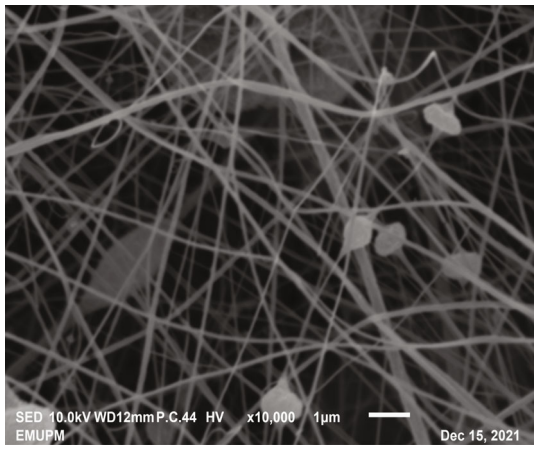

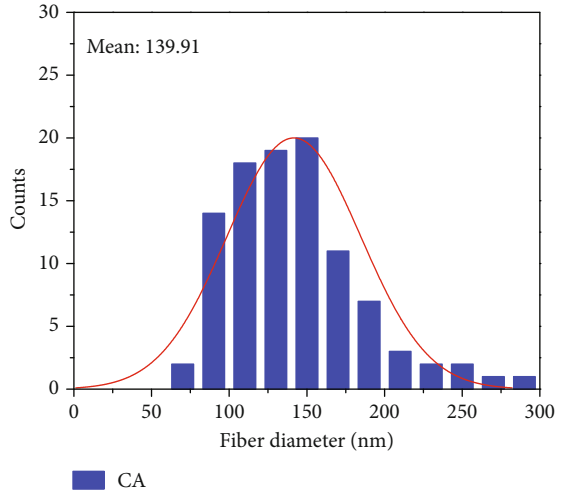

(a) CA

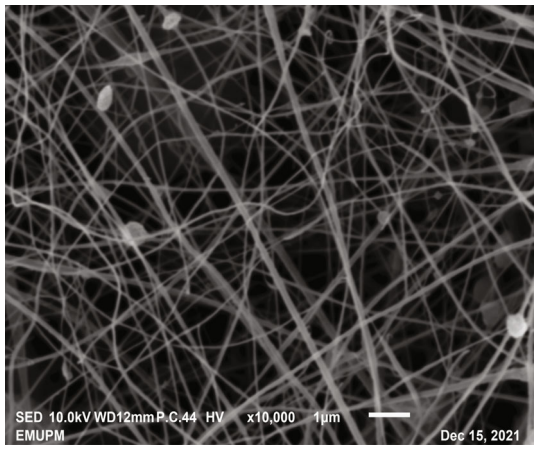

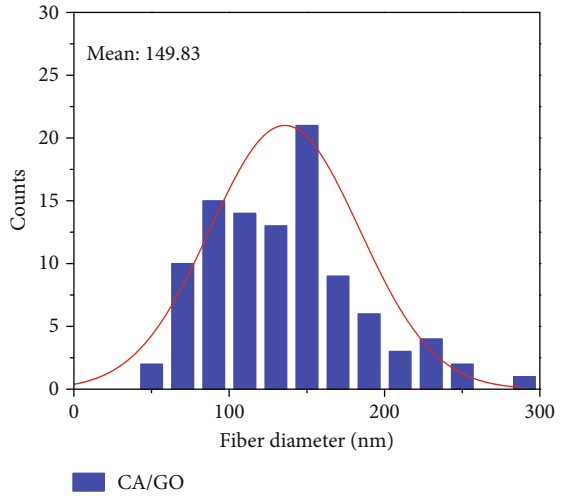

(b) CA/GO

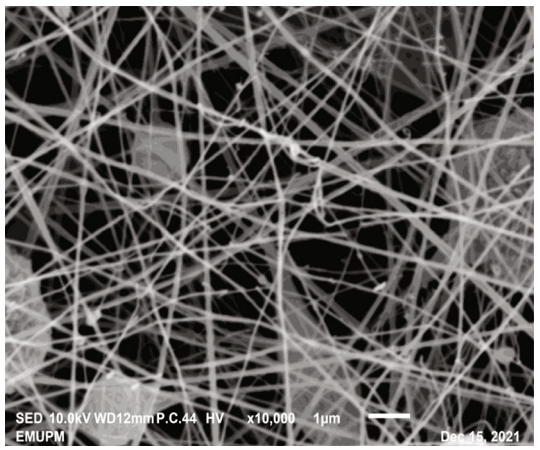

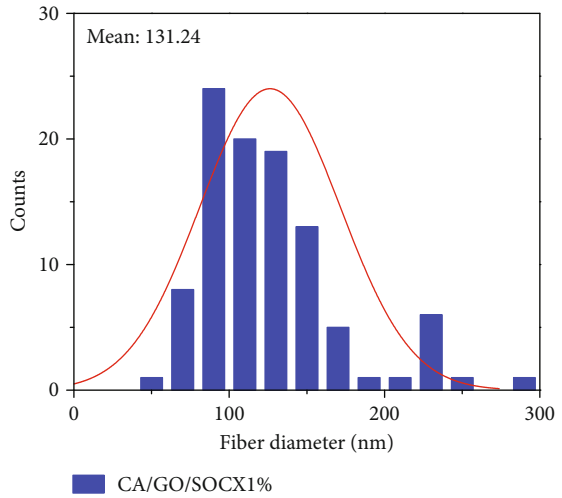

(c) CA/GO/SOCX1%

Figure 4: Continued.

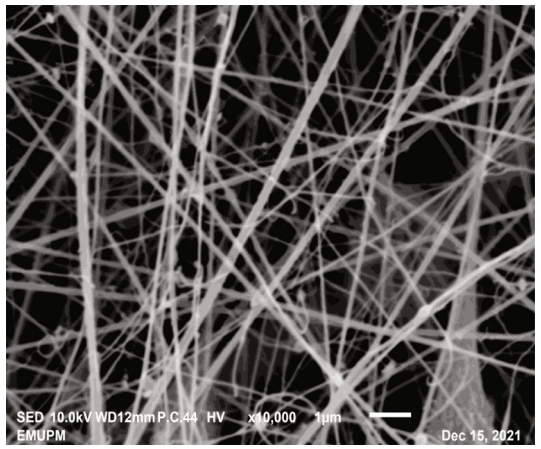

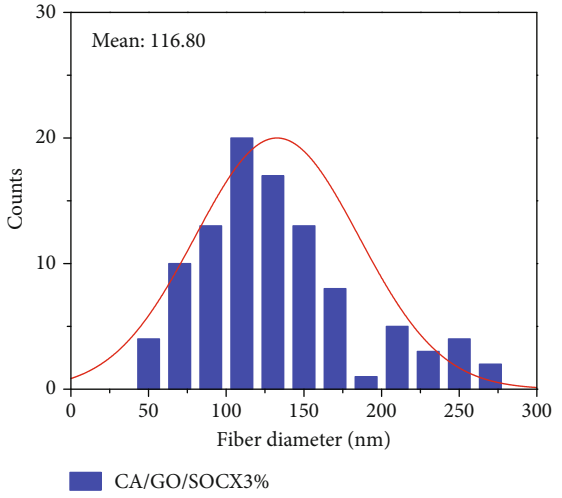

(d) CA/GO/SOCX3%

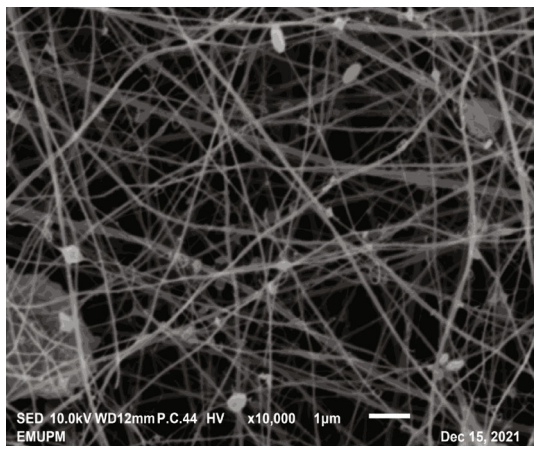

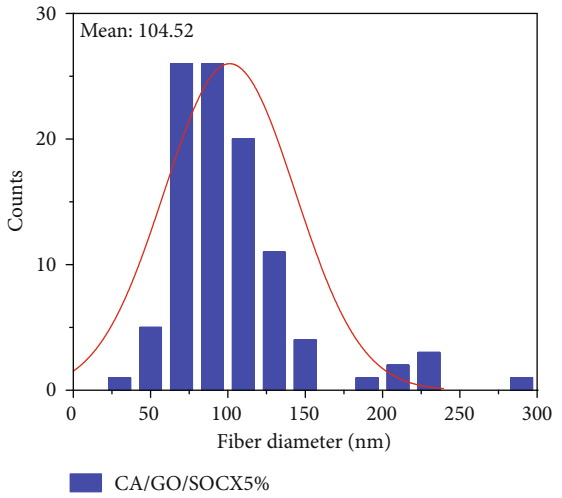

(e) CA/GO/SOCX5%

Figure 4: SEM micrograph of (a) CA nanofiber and (b) CA functionalized GO nanofiber, CA functionalized GO with (c) 1% p-SOCX, (d) 3% p-SOCX, and (e) 5% p-SOCX. 10000X magnification.

$$\%R : \frac{(C_o - C_e)}{C_o} \times 100. \tag{2}$$

C_o is the initial MB dye concentration (ppm); C_e is the equilibrium MB dye concentration (ppm); V is the volume of MB dye solution (L), and m is the dry mass of the adsorbent (g) [20].

2.5. Effect of Temperature. To study the effect of temperature, MB adsorption was carried out at 273 K, 338 K, and 358 K at 10 ppm MB concentration for 30 minutes. By using Equations (3)–(5), the thermodynamic parameters, namely, equilibrium constant: K_L, enthalpy change: ΔH, entropy change: ΔS, and Gibbs free energy: ΔG were determined. R is the gas constant ($8.314 \text{Jmol}^{-1}\text{K}^{-1}$) and T is the temperature in Kelvin (K).

$$K_L = \frac{C_o - C_e}{C_e}, \tag{3}$$

$$\ln K_L : \frac{\Delta S}{R} - \frac{\Delta H}{R} \cdot \frac{1}{T}, \tag{4}$$

$$\Delta G = \Delta H - T\Delta S. \tag{5}$$

3. Results and Discussion

3.1. FTIR Spectroscopy Analysis. Representative IR peaks of starting materials were observed in the nanofiber composite which attest to the successful process of integrating the materials. In general, FTIR spectra for CA closely resembles the composite nanofiber (CA/GO/SOCX 1%) albeit with slight shifting and differences in peak intensity as shown in Figures 3(a) and 3(b). Broad absorption peaks at around $3400\,\text{cm}^{-1}$ due to O–H stretching vibrations are discernible in all samples. Sharp absorption peak at $1740\,\text{cm}^{-1}$ followed by a small shoulder at $1724\,\text{cm}^{-1}$ attributed to C=O and C=C aromatic stretching vibrations are observed in all CA containing samples [21]. Therefore, mentioned C=C absorption peaks were also observed in the FTIR spectra of GO, *p*-

SOCX, and the composite [22]. Likewise, other main absorption bands of CA which are also present in GO and *p*-SOCX namely, C–O and CH_2 vibration was observed at 1040 cm^{-1} and 1428 cm^{-1}, respectively. Absorption peaks attributed to S=O stretching vibrations at 1200 cm^{-1} and 1050 cm^{-1} were also observed for SOCX and the composite nanofiber [23]. Thus, it can be concluded that GO and *p*-SOCX has been successfully integrated inside the nanofiber.

3.2. SEM Analysis. SEM images of the CA/GO nanofibers with different concentration of *p*-SOCX (1%, 3%, and 5%) are as shown in Figure 4. Smooth and uniform CA nanofibers was obtained with average fiber diameter of 300 ± 100 nm. After incorporating with GO, thin layer sheets were observed, and the fiber diameter was reduced to 200 ± 100 nm compared to CA nanofiber. This suggests that the size of nanofiber can possibly be controlled by introducing GO [24]. Furthermore, noticeable changes in morphology can be observed with changes in *p*-SOCX content, at higher concentration of *p*-SOCX, increase in the fiber diameter was observed, possibly due to the higher solution viscosity [25]. It is also clear that before adding *p*-SOCX, there were less beads, and the nanofibers appears more randomly oriented (Figures 4(a) and 4(b)) compared to nanofibers containing *p*-SOCX where the surface of nanofiber was less smooth and contained more beads or aggregates due to viscosity of the solution and blockage of more pores of fibers (Figures 4(c)–4(e)) [16]. This, in turn, led to the inefficiency in maintaining the jet stretching towards the collector [7].

3.3. XRD Analysis. XRD patterns in Figure 5 of CA exhibits typical cellulose acetate peaks at 14.16° and 21.06°, indicating a semicrystalline and amorphous phase of the CA nanofiber, respectively [26, 27]. On the other hand, CA/GO sample shows the major diffraction peak at 21.06° in which the CA peak intensity decreased indicating the successful incorporation of GO in CA nanofiber [24, 28]. In addition, the lower intensity reflections could be assigned to the other constituents as the weak broad peaks at the 2θ of 10°, 14°, and 21° were attributed to the amorphous structure, which relates to *p*-SOCX, CA, and GO components, respectively [27]. Hence, the XRD pattern provided a binary structure for prepared nanocomposite based on crystallinity and amorphous properties [29]. The XRD patterns of the CA/GO/SOCX materials exhibit a prominent peak around $2\theta = 10\circ$ indicating that the ordered structure's structural integrity is not significantly impacted by the modification process. This might be because the organic moieties inside the channels have a different scattering contrast from the amorphous silicate framework [30]. The same peak was also observed in the diffraction patterns of CA/GO and CA/GO with *p*-SOCX functionalization which indicated that the addition of *p*-SOCX did not change the crystalline structure of CA nanofibers.

3.4. TGA Analysis. Thermogravimetric analysis was carried out to study the compositions thermal stability; the results are displayed in Figure 6. Three stages of nanofiber degradation occurred in succession, from 50 to 300°C, 300 to 400°C,

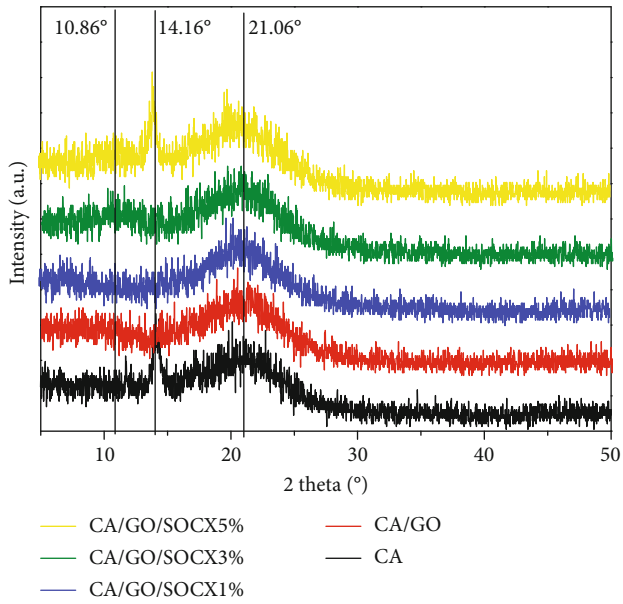

Figure 5: XRD diffractograms for nanofibers of CA, CA/GO, and CA/GO functionalized with 1%, 3%, and 5% *p*-SOCX.

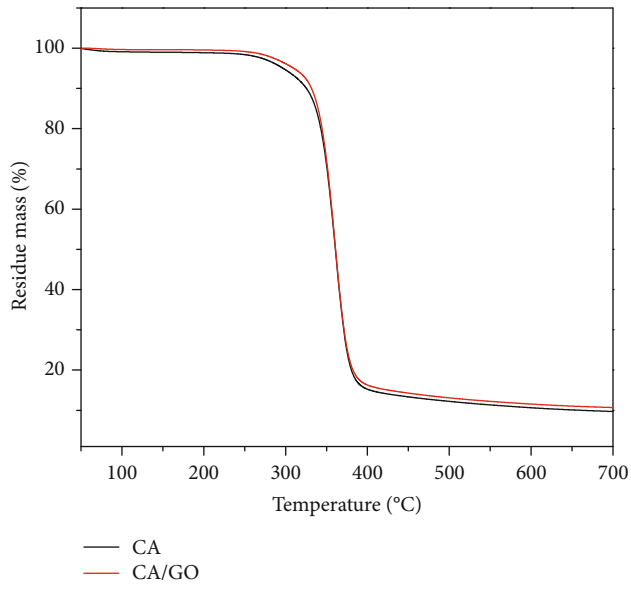

Figure 6: TGA Curves of CA nanofiber and CA with GO nanofiber at temperature between 50°C to 700°C.

and 400 to 700°C. [31]. The initial step considered weight loss, moisture loss from the material, and solvent residue from the electrospinning process. The weight loss of pure CA nanofibers from 242 to 327°C was attributed to the degradation of bulk CA while CA/GO nanofiber weight loss start from 263 to 328°C due to the removal of different oxygen containing functional group on GO surface and thermal pyrolysis of the cellulose skeleton within this temperature range [32–34]. The moisture content in the CA is 8% while 5% for CA/GO based on the initial weight loss as the lingering solvents from the CA electrospinning solution may be responsible for the small weight loss variation between the

Table 1: CHNS elemental analysis of CA, GO functionalized CA nanofiber, and GO and p-SOCX functionalized CA nanofiber at different amount of p-SOCX (1%,3%, and 5%).

Sample	Carbon %		Hydrogen %		Oxygen %		Sulphur %	
	Calc.	Exp.	Calc.	Exp.	Calc.	Exp.	Calc.	Exp.
CA	46.88	46.81	5.00	5.34	48.12	47.85	0	0
CA/GO	45.40	47.37	6.07	5.83	48.53	46.80	0	0
CA/GO/SOCX 1%	45.43	49.56	6.03	5.57	48.37	44.47	0.17	0.37
CA/GO/SOCX 3%	45.46	52.06	5.94	5.82	48.08	41.55	0.52	0.49
CA/GO/SOCX 5%	45.43	49.53	5.90	5.49	47.81	44.19	0.86	0.71

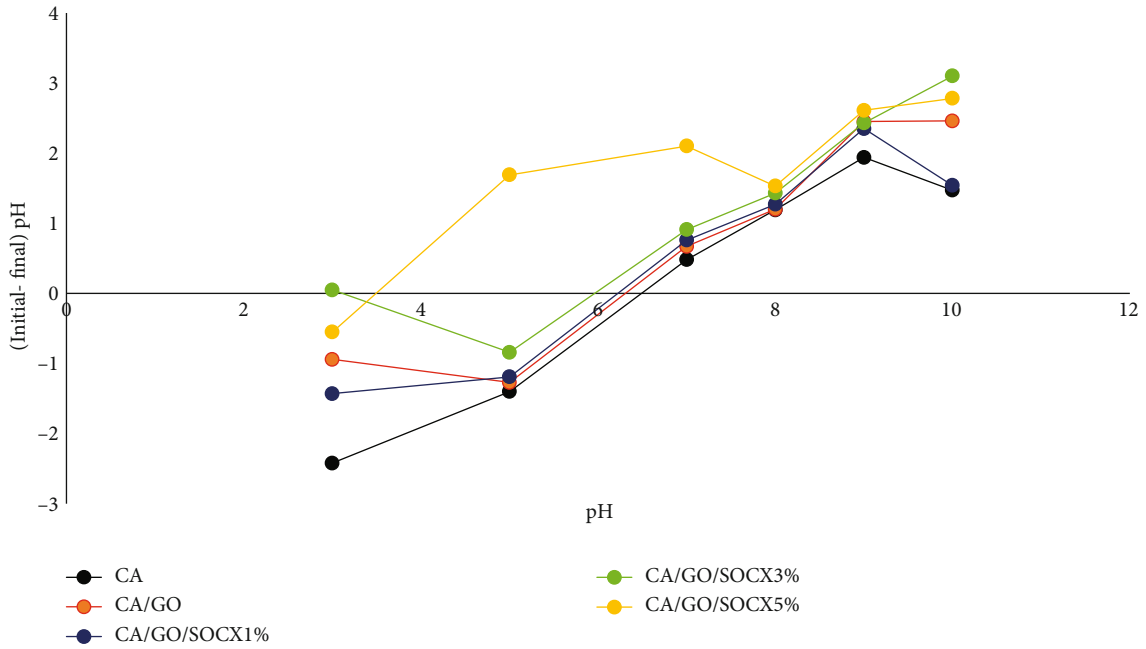

Figure 7: pH of point of zero charge (pH_{PZC}) for CA, GO functionalized CA nanofiber, and GO functionalized CA with different *p*-SOCX loading (1%, 3%, and 5%). Conditions for pH_{PZC} study, 0.5 ml of 0.1 M $NaNO_3$ solution, 25 mg/L of adsorbent dosage and 24 hours contact time with pH variation (3, 5, 7, 8, 9, and 10).

electrospun nanofibers [16, 35]. Noteworthy mentioning, CA/GO exhibits slightly better thermal stability compared to CA based on the weight loss behavior observed at 300°C to 350°C, thus suggesting that GO imparts thermal stability to the nanofiber. Both compositions experienced an exponential increase in the rate of weight loss, which peaked at 92% for CA and 95% for CA/GO nanofibers. [17]. de Almeida et al., reported that the third stage occurs above 400°C, where the entire degradation of the nanofiber occurs, leaving a little amount of residues for materials containing CA [21].

3.5. Elemental Analysis. The elemental analysis results of CA, CA/GO, and CA/GO/SOCX (1%, 3%, and 5%) are as shown in Table 1. Results show that the experimentally determined percentage of carbon, hydrogen, and sulphur are close to the calculated values. An increase in sulphur content was observed with increase in *p*-SOCX loading (Table 1). Nevertheless, differences in values may occur due to presence of impurities originating from the solvents that are used to dissolve the polymer solution prior to the fiber making process. In conclusion, it can be confirmed that both GO and *p*-SOCX are successfully integrated into the nanofiber.

3.6. Effect of pH, and Adsorbent Dosage. Since pH may give rise to ionization of the adsorbate, pH_{PZC} value for the adsorbents was determined. The pH_{PZC} value and the effect of pH towards MB removal for all samples are as shown in Figures 7 and 8(a), respectively. As shown in Figure 7, a pronounced effect of pH towards the adsorbate's surface charge can be observed from the adsorption performance at pH 3 up to pH 10. The pH_{PZC} obtained for CA, CA/GO, CA/GO/SOCX 1%, and CA/GO/SOCX 3% is between pH 6.0-6.5, while for CA/GO/SOCX 5%, is around pH 3.5. In general, at $pH < pH_{PZC}$ the surface of the adsorbent can be considered as positively charged, while beyond pH_{PZC} values, the surface becomes negatively charged. Therefore, at $pH < pH_{PZC}$ there is possibility of electrostatic repulsion forces between the adsorbent surface and MB and which may result in lower adsorption performance [20].

MB removal at pH below than 7 was insignificant, possibly due to at lower pH values i.e., acidic, the electrostatic

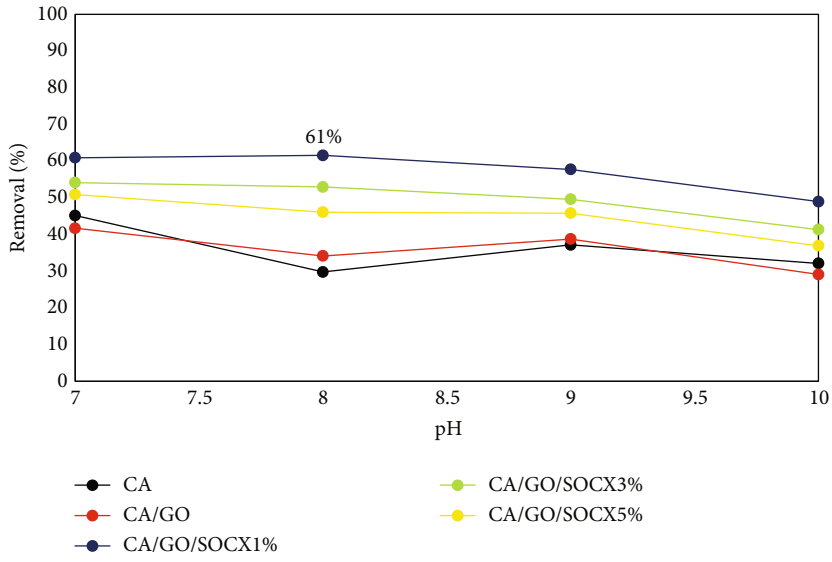

(a)

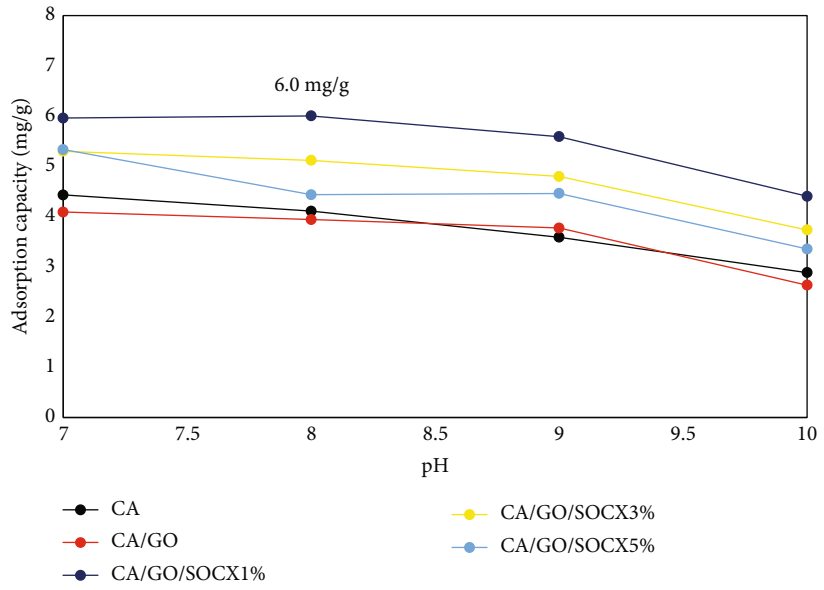

(b)

Figure 8: Continued.

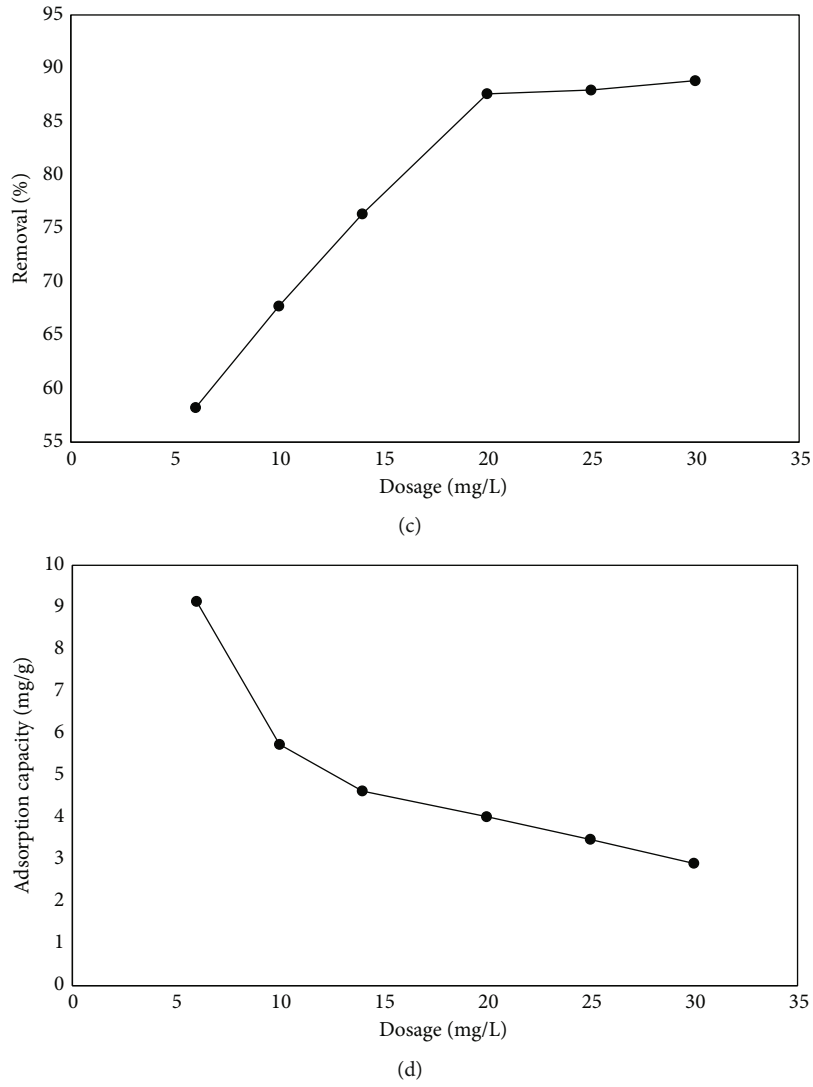

Figure 8: Study on effect of pH towards MB removal (a) and adsorption capacity (b) for all nanofibers (CA, GO functionalized CA nanofiber, and GO functionalized CA with SOCX 1%,3%, and 5%). Static adsorption condition for pH study, dosage 6 mg/L, concentration 10 ppm, and contact time 30 minutes. Effect of adsorbent dosage towards MB removal (c) and adsorption capacity (d) for GO functionalized CA with 1% of SOCX. Static adsorption condition for dosage study, pH 8 concentration 10 ppm, and contact time 30 minutes.

repulsion between protonated adsorption sites on the adsorbents and the protonated dimethylamine group in MB limits the interaction and results in low adsorption capacity [36]. However, upon increasing pH, deprotonation of sulfonate group takes place, generating negative surface charge on *p*-SOCX leading to arising electrostatic interactions between MB and *p*-SOCX molecules, thus, favoring the adsorption process [37, 38]. Herein, a maximum adsorption of 61% and the adsorption capacity *ca.* 6 mg/g at pH 8 for CA/GO/SOCX 1% sample was obtained (Figure 8(a)). Meanwhile, at high pH i.e., pH > 8, adsorption capacity decreased, possibly due to the deprotonation of carboxylic acid and hydroxyl groups giving rise to repulsion with nitrogen in MB [39, 40].

Based on the best adsorption performance exhibited by CA/GO/SOCX 1% nanofiber, it was selected for the study on effect of dosage. Herein the amount of CA/GO/SOCX 1% was varied between 6 to 30 mg (Figures 8(c) and 8(d)). Figure 6(c) shows that below 20 mg adsorbent, the removal percentage exhibits a steady increase along with an increase in the amount of adsorbent, indicating an increase in available adsorptive surface sites. However, at 20 mg and above, a plateau is observed which indicates equilibrium i.e., saturation of adsorptive sites. Meanwhile, adsorption capacity decreased with an increase in adsorbent dosage amount due to an increase in interaction between active sites of nanofibrous adsorbents with a fixed amount of MB molecules available [41].

Other similar adsorbents which incorporate calixarene for MB removal have also been reported elsewhere. For instance, Kamboh et al., reported that 94% of MB removal was recorded for *p*-sulphonatocalix[8]arene-based silica resin at pH 9.5 at adsorbent dosage of 40 mg/L [13]. Meanwhile, in another study, calix[8]arene modified sulphur exhibited >90% MB removal at pH 6 with adsorbent dosage

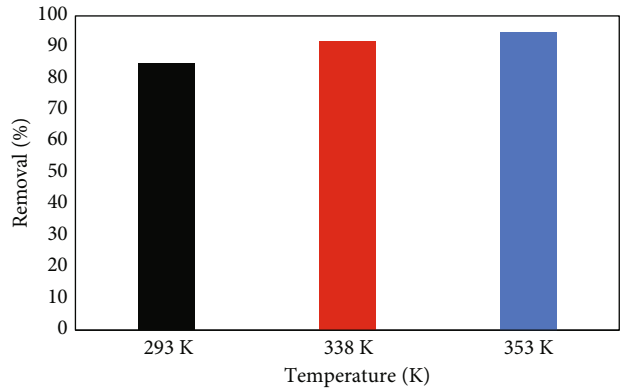

Figure 9: MB removal at different temperatures (293 K, 338 K, and 353 K) with static adsorption condition: pH = 8, dosage = 20 mg/L, concentration = 10 ppm, and contact time = 30 minutes.

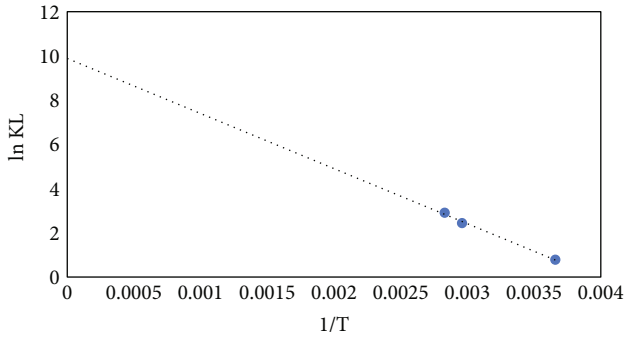

Figure 10: Van't Hoff plot for evaluating the thermodynamic parameters of MB adsorption by GO functionalized CA with 1% *p*-SOCX. Static adsorption condition: pH 8, dosage 20 mg/L, concentration 10 ppm, and contact time 30 minutes.

Table 2: Thermodynamic parameters for MB adsorption onto GO functionalized CA with 1% *p*-SOCX.

Temp. (K)	Removal %	K_L	ΔG (kJ/Mol)	ΔH (kJ/Mol)	ΔS (J/Mol.K)	$R2$
293	85	2.18	-1.77			
338	92	11.38	-6.83	2.066	82.07	0.989
353	95	18.25	-8.52			

of 45 mg/L and 180 minutes contact time [42]. Silica gel supported dinitro calix[4]arene cage, was reported to achieve 93% MB removal at pH 12 with 0.05 mg/L of adsorbent dosage and 120 minutes contact time. [23]. On the other hand, the adsorbent developed in this study i.e., CA/GO/SOCX 1% has the ability to remove up to 88.84% of MB at 20 mg/L adsorbent dosage in 30 minutes. Noteworthy mentioning that, only small amount of adsorbent is needed to remove the MB and with shorter time by using CA/GO/SOCX 1% compared to other adsorbents mentioned above.

3.7. Effect of Temperature. Results shown in Figure 9 indicates that adsorption is promoted with increase in temperature, where an 85% removal at 293 K increased to 92% at 338 K followed by 95% at 353 K. This increase in adsorption efficiency with temperature suggests an endothermic nature of the adsorption process, i.e., chemisorption [43]. The change in free energy (ΔG_o) was calculated and evaluated together with the change in enthalpy (ΔH_o) and entropy (ΔS_o) from the Van't Hoff plot in Figure 10, and summary is given in Table 2. Negative values of ΔG_o indicates feasibility and spontaneity of MB adsorption onto the adsorbent. While the positive value of ΔSo (82.07 J/mol.K) indicates an increase in degree of freedom of the adsorbing system with spontaneity [44].

4. Conclusion

CA/GO/SOCX nanofiber was successfully prepared using the electrospinning technique featuring superior MB dye removal efficiency compared to CA and CA/GO alone. SEM, FTIR, XRD, TGA, and CHNS analyses confirmed the presence of CA, GO, and *p*-SOCX in the nanofiber sample obtained. SEM images also showed that the fibers diameter web increased within increase in *p*-SOCX loading. The optimum dye removal conditions, i.e., pH and dosage were established at pH 8 and 20 mg/L, respectively. Best adsorption capacity was shown by CA/GO/SOCX 1% nanofiber sample with 4 mg/g adsorption capacity and 88.84% MB removal.

Data Availability

The authors confirm that all data generated or analyzed during this study are available from the corresponding author. These materials can be requested directly from the corresponding author if needed.

Conflicts of Interest

The authors declared no conflict of interest with respect to the research, authorship, and publication of this article.

Acknowledgments

Authors would like to thank the Ministry of Education Malaysia for funding this study, through grant no: FRGS/1/2018/STG01/UPM/02/11.

References

[1] H. A. Altaleb, B. M. Thamer, M. M. Abdulhameed, H. El-Hamshary, S. Z. Mohammady, and A. M. Al-Enizi, "Efficient electrospun terpolymer nanofibers for the removal of cationic dyes from polluted waters: a non-linear isotherm and kinetic study," *Journal of Environmental Chemical Engineering*, vol. 9, no. 4, article 105361, 2021.

[2] A. Siciliano, G. M. Curcio, C. Limonti, S. Masi, and M. Greco, "Methylene blue adsorption on thermo plasma expanded graphite in a multilayer column system," *Journal of Environmental Management*, vol. 296, article 113365, 2021.

[3] A. A. Elzain, M. R. El-Aassar, F. S. Hashem, F. M. Mohamed, and A. S. M. Ali, "Removal of methylene dye using composites of poly (styrene- *co* -acrylonitrile) nanofibers impregnated with adsorbent materials," *Journal of Molecular Liquids*, vol. 291, article 111335, 2019.

[4] S. Tahazadeh, H. Karimi, T. Mohammadi, H. B. M. Emrooz, and M. A. Tofighy, "Fabrication of biodegradable cellulose acetate/MOF-derived porous carbon nanocomposite adsorbent for methylene blue removal from aqueous solutions," *Journal of Solid State Chemistry*, vol. 299, article 122180, 2021.

[5] M. R. R. Kooh, R. Thotagamuge, Y.-F. C. Chau, A. H. Mahadi, and C. M. Lim, "Machine learning approaches to predict adsorption capacity of Azolla pinnata in the removal of methylene blue," *Journal of the Taiwan Institute of Chemical Engineers*, vol. 132, article 104134, 2022.

[6] R. Lyu, C. Zhang, T. Xia et al., "Efficient adsorption of methylene blue by mesoporous silica prepared using sol-gel method employing hydroxyethyl cellulose as a template," *Colloids and Surfaces A: Physicochemical and Engineering Aspects*, vol. 606, article 125425, 2020.

[7] W. Chen, H. Ma, and B. Xing, "Electrospinning of multifunctional cellulose acetate membrane and its adsorption properties for ionic dyes," *International Journal of Biological Macromolecules*, vol. 158, pp. 1342–1351, 2020.

[8] R. Lafi, I. Montasser, and A. Hafiane, "Adsorption of Congo red dye from aqueous solutions by prepared activated carbon with oxygen-containing functional groups and its regeneration," *Adsorption Science & Technology*, vol. 37, no. 1-2, pp. 160–181, 2019.

[9] S. Soudagar, S. Akash, M. S. Venkat, V. R. Poiba, and M. Vangalapati, "Adsorption of methylene blue dye on nano graphene oxide-thermodynamics and kinetic studies," *Materials Today: Proceedings*, vol. 59, pp. 667–672, 2022.

[10] N. Z. Rosly, A. H. Abdullah, M. Ahmad Kamarudin, S. E. Ashari, and S. A. Alang Ahmad, "Adsorption of methylene blue dye by calix[6]arene-modified lead sulphide (Pbs): optimisation using response surface methodology," *International Journal of Environmental Research and Public Health*, vol. 18, no. 2, p. 397, 2021.

[11] B. B. Adhikari, M. Kanemitsu, H. Kawakita, K. O. Jumina, and K. Ohto, "Synthesis and application of a highly efficient polyvinylcalix[4]arene tetraacetic acid resin for adsorptive removal of lead from aqueous solutions," *Chemical Engineering Journal*, vol. 172, no. 1, pp. 341–353, 2011.

[12] S. A. Fahmy, J. Brüßler, F. Ponte et al., "A study on the physicochemical properties and cytotoxic activity of p-sulfocalix[4]-arene-nedaplatin complex," *Journal of Physics: Conference Series*, vol. 1310, no. 1, article 012011, 2019.

[13] M. A. Kamboh, W. A. W. Ibrahim, H. R. Nodeh, L. A. Zardari, S. T. H. Sherazi, and M. M. Sanagi, "p-sulphonatocalix[8]arene functionalized silica resin for the enhanced removal of methylene blue from wastewater: equilibrium and kinetic study," *Separation Science and Technology*, vol. 54, no. 14, pp. 2240–2251, 2019.

[14] M. Chen, C. Wang, W. Fang et al., "Electrospinning of calixarene-functionalized polyacrylonitrile nanofiber membranes and application as an adsorbent and catalyst support," *Langmuir*, vol. 29, no. 38, pp. 11858–11867, 2013.

[15] F. Özcan, M. Bayrakcı, and Ş. Ertul, "Synthesis and characterization of novel nanofiber based calixarene and its binding efficiency towards chromium and uranium ions," *Journal of Inclusion Phenomena and Macrocyclic Chemistry*, vol. 85, no. 1-2, pp. 49–58, 2016.

[16] A. ZabihiSahebi, S. Koushkbaghi, M. Pishnamazi, A. Askari, R. Khosravi, and M. Irani, "Synthesis of cellulose acetate/chitosan/SWCNT/Fe3O4/TiO2 composite nanofibers for the removal of Cr(VI), As(V), methylene blue and Congo red from aqueous solutions," *International Journal of Biological Macromolecules*, vol. 140, pp. 1296–1304, 2019.

[17] G. El-Barbary, M. K. Ahmed, M. M. El-Desoky et al., "Cellulose acetate nanofibers embedded with Ag nanoparticles/CdSe/graphene oxide composite for degradation of methylene blue," *Synthetic Metals*, vol. 278, article 116824, 2021.

[18] G. Sargazi, D. Afzali, A. Mostafavi, and S. Y. Ebrahimipour, "Synthesis of CS/PVA biodegradable composite nanofibers as a microporous material with well controllable procedure through electrospinning," *Journal of Polymers and the Environment*, vol. 26, no. 5, pp. 1804–1817, 2018.

[19] A. A. Aly and M. K. Ahmed, "Nanofibers of cellulose acetate containing ZnO nanoparticles/graphene oxide for wound healing applications," *International Journal of Pharmaceutics*, vol. 598, article 120325, 2021.

[20] N. S. Abdul Mubarak, N. N. Bahrudin, A. H. Jawad, B. H. Hameed, and S. Sabar, "Microwave enhanced synthesis of sulfonated chitosan-montmorillonite for effective removal of methylene blue," *Journal of Polymers and the Environment*, vol. 29, no. 12, pp. 4027–4039, 2021.

[21] D. S. De Almeida, E. H. Duarte, E. M. Hashimoto et al., "Development and characterization of electrospun cellulose acetate nanofibers modified by cationic surfactant," *Polymer Testing*, vol. 81, article 106206, 2020.

[22] M. M. Ibrahim, T. Y. Fahmy, E. I. Salaheldin, F. Mobarak, M. A. Youssef, and M. R. Mabrook, "Role of tosyl cellulose acetate as potential carrier for controlled drug release," *Life Science Journal*, vol. 10, no. 12, pp. 127–133, 2015.

[23] F. Temel, M. Turkyilmaz, and S. Kucukcongar, "Removal of methylene blue from aqueous solutions by silica gel supported calix[4]arene cage: investigation of adsorption properties," *European Polymer Journal*, vol. 125, article 109540, 2020.

[24] J. Prakash, K. S. Venkataprasanna, G. Bharath, F. Banat, R. Niranjan, and G. D. Venkatasubbu, "In-vitro evaluation of electrospun cellulose acetate nanofiber containing graphene oxide/TiO2/curcumin for wound healing application," *Colloids and Surfaces a: Physicochemical and Engineering Aspects*, vol. 627, article 127166, 2021.

[25] M. Keskinates, B. Yilmaz, Y. Ulusu, and M. Bayrakci, "Electrospinning of novel calixarene-functionalized PAN and PMMA nanofibers: comparison of fluorescent protein adsorption performance," *Materials Chemistry and Physics*, vol. 205, pp. 522–529, 2018.

[26] L. Jia, X. Huang, H.'. Liang, and Q. Tao, "Enhanced hydrophilic and antibacterial efficiencies by the synergetic effect TiO_2 nanofiber and graphene oxide in cellulose acetate nanofibers," *International Journal of Biological Macromolecules*, vol. 132, pp. 1039–1043, 2019.

[27] R. Al-Wafi, M. K. Ahmed, and S. F. Mansour, "Tuning the synthetic conditions of graphene oxide/magnetite/ hydroxyapatite/cellulose acetate nanofibrous membranes for removing Cr(VI), Se(IV) and methylene blue from aqueous solutions," *Journal of Water Process Engineering*, vol. 38, article 101543, 2020.

[28] A. Salama, "New sustainable hybrid material as adsorbent for dye removal from aqueous solutions," *Journal of Colloid and Interface Science*, vol. 487, pp. 348–353, 2017.

[29] S. Rezania, M. A. Kamboh, S. S. Arian et al., "Nitrile-calixarene grafted magnetic graphene oxide for removal of arsenic from aqueous media: isotherm, kinetic and thermodynamic studies," *Chemosphere*, vol. 268, article 129348, 2021.

[30] S. M. Alahmadi, S. Mohamad, and M. J. Maah, "Synthesis and characterization of mesoporous silica functionalized with calix[4]arene derivatives," *International Journal of Molecular Sciences*, vol. 13, no. 12, pp. 13726–13736, 2012.

[31] M. Arumugam, B. Murugesan, N. Pandiyan, D. K. Chinnalagu, G. Rangasamy, and S. Mahalingam, "Electrospinning cellulose acetate/silk fibroin/Au-Ag hybrid composite nanofiber for enhanced biocidal activity against MCF-7 breast cancer cell," *Materials Science and Engineering: C*, vol. 123, article 112019, 2021.

[32] R. Li, J. Dou, Q. Jiang et al., "Preparation and antimicrobial activity of β-cyclodextrin derivative copolymers/cellulose acetate nanofibers," *Chemical Engineering Journal*, vol. 248, pp. 264–272, 2014.

[33] N. M. Aboamera, A. Mohamed, A. Salama, T. A. Osman, and A. Khattab, "An effective removal of organic dyes using surface functionalized cellulose acetate/graphene oxide composite nanofibers," *Cellulose*, vol. 25, no. 7, pp. 4155–4166, 2018.

[34] H. Zang, Y. Li, Y. Li et al., "Adsorptive removal of cationic dye from aqueous solution by graphene oxide/cellulose acetate composite," *Journal of Nanoscience and Nanotechnology*, vol. 19, no. 8, pp. 4535–4542, 2019.

[35] S. Beikzadeh, A. Akbarinejad, S. Swift, J. Perera, P. A. Kilmartin, and J. Travas-Sejdic, "Cellulose acetate electrospun nanofibers encapsulating _lemon myrtle_ essential oil as active agent with potent and sustainable antimicrobial activity," *Reactive and Functional Polymers*, vol. 157, article 104769, 2020.

[36] M. A. Zulfikar, D. Maulina, M. Nasir, N. Handayani, and M. Handajani, "Removal of methylene blue from aqueous solution using poly(acrylic acid)/SiO_2 and functionalized poly(acrylic acid)/SiO_2 composite nanofibers," *Environmental Nanotechnology, Monitoring & Management*, vol. 14, article 100381, 2020.

[37] S. Çetintaş, "An alternative application for reuse of leaching residues: determination of adsorption behaviour for methylene blue and process optimization," *Sustainable Chemistry and Pharmacy*, vol. 23, article 100504, 2021.

[38] A. S. Ibupoto, U. A. Qureshi, F. Ahmed et al., "Reusable carbon nanofibers for efficient removal of methylene blue from aqueous solution," *Chemical Engineering Research and Design*, vol. 136, pp. 744–752, 2018.

[39] Z. Yang, X. Liu, X. Liu et al., "Preparation of β-cyclodextrin/graphene oxide and its adsorption properties for methylene blue," *Colloids and Surfaces. B, Biointerfaces*, vol. 200, article 111605, 2021.

[40] R. Zhao, Y. Wang, X. Li, B. Sun, and C. Wang, "Synthesis of β-cyclodextrin-based electrospun nanofiber membranes for highly efficient adsorption and separation of methylene blue," *ACS Applied Materials & Interfaces*, vol. 7, no. 48, pp. 26649–26657, 2015.

[41] T. Subbiah, G. S. Bhat, R. W. Tock, S. Parameswaran, and S. S. Ramkumar, "Electrospinning of nanofibers," *Journal of Applied Polymer Science*, vol. 96, no. 2, pp. 557–569, 2005.

[42] N. Z. Rosly, S. Ishak, A. H. Abdullah, M. A. Kamarudin, S. E. Ashari, and S. A. A. Ahmad, "Fabrication and optimization calix[8]arene-PbS nanoadsorbents for the adsorption of methylene blue: isotherms, kinetics and thermodynamics studies," *Journal of Saudi Chemical Society*, vol. 26, no. 1, article 101402, 2022.

[43] L. Boughrara, F. Zaoui, M.'. Guezzoul, F. Z. Sebba, B. Bounaceur, and S. O. Kada, "New alginic acid derivatives ester for methylene blue dye adsorption: kinetic, isotherm, thermodynamic, and mechanism study," *International Journal of Biological Macromolecules*, vol. 205, pp. 651–663, 2022.

[44] M. Duhan and R. Kaur, "Phytic acid doped polyaniline nanofibers: an advanced adsorbent for methylene blue dye," *Environmental Nanotechnology, Monitoring & Management*, vol. 12, article 100248, 2019.